Rheo-Optical Evidence of a Flow-Induced Isotropic−Nematic Transition in a Thermotropic Liquid-Crystalline Polymer

Patrick T. Mather,*,† Angel Romo-Uribe,‡ Chang Dae Han,*,§,∥ and Seung Su Kim§

Wright Laboratory, Materials Directorate, and Systran Corporation, WL/MLBP, 2941 P Street Suite 1, Wright Patterson AFB, Ohio 45433-7750, and Department of Polymer Engineering, The University of Akron, Akron, Ohio 44325-0301

Received May 27, 1997; Revised Manuscript Received August 21, 1997[⊗]

ABSTRACT: A direct rheo-optical characterization of the flow-induced isotropic−nematic (I−N) transition in a semiflexible thermotropic liquid-crystalline polymer (TLCP) was investigated, using a specially constructed apparatus enabling in-situ optical microscopic observations at elevated temperatures, along with cone-and-plate rheometry. For the investigation, an aromatic polyester, poly[(phenylenesulfonyl)-*p*-phenylene 1,10-decamethylenebis(4-oxybenzoate)] (PSHQ10), was synthesized via solution polymerization. Above the equilibrium isotropic−nematic transition temperature for this polymer, $T = 170.5$ °C, application of steady-state shear flow above a certain critical value of shear rate, $\dot{\gamma}_c$, produces a first-order I−N transition, with $\dot{\gamma}_c$ increasing with temperature. This transition is evidenced by the formation of elongated nematic (birefringent) domains in the isotropic matrix, accompanied by a drastic decrease in shear viscosity (η). Remarkably, the nematic domains that form for $\dot{\gamma} > \dot{\gamma}_c$ are optically uniform under cross-polarized optical microscopy; i.e., they are apparently free of disclinations (defects), typical of textured TLCPs. The flow-induced I−N transition in PSHQ10 is found to be reversible; i.e., upon cessation of shear flow, the domains melt to the original isotropic phase and the dynamic moduli rise toward the pretransition values. The observed flow-induced I−N transition may find important applications, such as envisaging new routes for processing TLCPs with better mechanical properties and helping to understand bioprocesses such as silk thread spinning.

Introduction

Flow-induced phase transition in polymer systems has been an active research area where several important processes such as flow-induced crystallization[1] and flow-induced mixing and demixing effects in polymer solutions and melts have been studied experimentally[2−5] and theoretically.[6] There is a general agreement among researchers that crystallization is facilitated when a polymer solution or melt is subjected to a flow field. However, regarding the effect of a flow field on phase transition in mixtures of polymer and solvent or in mixtures of two polymers either in solution or in the molten state, there are two opposing experimental observations reported in the literature. Experimental evidence has shown that application of shearing promotes phase separation (i.e., the shear-induced demixing effect).[3−5] Such experimental observations are predicted by theory.[6,7] On the contrary, other research workers have presented experimental evidence that homogenization (i.e., flow-induced mixing effect) is promoted when a two-phase mixture of polymers is subjected to a shear flow field.[8−12] It should be noted that in some cases a reversed phase transition was observed after cessation of shearing.[3,8]

In recent years, liquid crystalline polymers (LCPs) have attracted much attention of polymer scientists.[13,14] These structured fluids display rich optical microstructures that arise from the anisotropy of the local structure, the variety of topological defects that can form in the liquid-crystalline mesophase, and the complex dynamics that give rise to texture evolution under flow.[15,16] While providing fertile ground for much intriguing materials physics, the structural complexities associated with the coupling of orientation and flow have proven to be factors limiting the ultimate properties of LCPs.[17−21] Thus, the rheological behavior of both thermotropic liquid-crystalline polymers (TLCPs)[22−31] and lyotropic LCPs[32−42] has been studied extensively.

Flow-induced disorder−order transitions in LCPs are of prime interest because such transitions may explain the origin of mechanical instabilities under processing conditions[7,43] and help to understand bioprocesses such as the function of cell membranes[44] and spider spinning processes.[45] Some theoretical treatments of lyotropic LCPs show that elongational flow[46] will promote isotropic−nematic (I−N) transition at a concentration below that predicted by the Flory theory[47] of rodlike molecules in the absence of a flow field; others predict that the nematic phase is more stable than the disordered isotropic one[48] or that the I−N transition can be induced by imposing a flow, if the shear rate exceeds a certain critical value, and the critical shear rate ($\dot{\gamma}_c$) will decrease with increasing concentration.[49] Despite this background, no reports exist of a flow-induced I−N transition in lyotropic LCPs.

We are interested primarily in flow-induced phase transitions, as they apply to technologically relevant thermotropic main-chain liquid crystalline polymers. However, a satisfactory understanding of the flow behavior of TLCPs even in the pure nematic state has remained largely elusive. The slow progress in this field is largely due to the lack of a suitable theory (rigid rod models must be extended to the "mixture" of rigidity and flexibility in real systems) and to the lack of model TLCPs. Recently, however, Han and Kim[50] presented results that suggest a shear-induced I−N transition in a semiflexible thermotropic polyester by measuring shear stress, and dynamic storage and loss moduli, upon application and following cessation of a steady shear flow.

† Wright Laboratory.
‡ Systran Corp.
§ The University of Akron.
∥ Present address: Hoechst Research and Technology, 86 Morris Ave, Summit, NJ 07901.
[⊗] Abstract published in *Advance ACS Abstracts,* November 15, 1997.

S0024-9297(97)00737-7 CCC: $14.00

Some theoretical progress has been made in describing the I−N transition in shearing flow of thermotropic nematics. Olmsted and Goldbart[51,52] have developed a generalized Leslie−Ericksen (LE) theory applicable to polymeric liquid crystals in the sense that it describes the evolution of a molecular orientation tensor, S_{ij} (rather than simply the director unit vector of LE theory), with respect to dimensionless shear rate and temperature. By examination of the effect of increasing shear rate on the temperature dependence of the nematic order parameter, it was found that, on cooling, steady shearing has the effect of suppressing the orientational fluctuations such that the nematic phase appears (on cooling) at temperatures increasing with increasing shear rate. Furthermore, their theory predicts that a nonequilibrium critical point should exist so that above a critical shear rate there is a continuous order parameter−temperature curve. While the results of these theoretical calculations agree qualitatively with experiment,[23,53] quantitative comparison has yet to be demonstrated.

In the present study, we demonstrate the existence of a flow-induced I−N transition in the same polymer as that employed in the previous study of Han and Kim.[50] For this we have used novel *in-situ* rheo-optical techniques,[54] in combination with cone-and-plate mechanical rheometry, enabling us to make *direct observation* of the flow-induced I−N transition in a TLCP.

Experimental Section

Materials. For the study, an aromatic polyester, poly-[(phenylenesulfonyl)-*p*-phenylene 1,10-decamethylenebis(4-oxybenzoate)], based on a triad ester mesogenic unit was synthesized. The mesogen contains an arylsulfonyl-substituted hydroquinone alternated with a decamethylene spacer.[55] The polymer, whose chemical formula is shown below, will be referred to as PSHQ10.

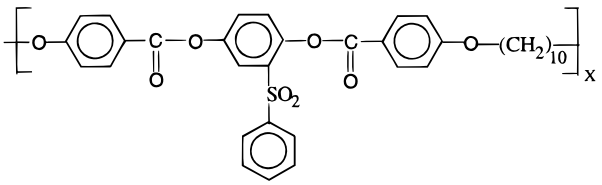

PSHQ10 was synthesized via solution polymerization, and the details of polymerization and characterization methods are given elsewhere.[56,57] The chemical structure was confirmed via two-dimensional, high-resolution nuclear magnetic resonance (NMR) spectroscopy.[57] Following a fractionation step for isolating high molecular weight species, the polymer has a weight-average molecular weight, as determined by size exclusion chromatography, of 45 000 relative to polystyrene standards, and a polydispersity index of about 2. Thermogravimetric measurements show that the polymer degrades at temperatures above $T = 350$ °C, well above its nematic−isotropic transition ("clearing") temperature (T_{NI}).

Sample Preparation. Specimens for rheo-optical and rheological characterization were prepared by first dissolving PSHQ10 in dichloromethane in the presence of an antioxidant (Irganox 1010, Ciba-Geigy Group) and then slowly evaporating the solvent at room temperature for 1 week. The cast films (1 mm thick) were further dried in a vacuum oven at room temperature for at least 3 weeks and, prior to measurements, at 90 °C for 48 h in order to remove any residual solvent and moisture.

Thermal Analysis. Thermal transition temperatures were determined by differential scanning calorimetry (DSC) with a Perkin-Elmer DSC Delta 7 series. Measurements were performed under a nitrogen atmosphere. Because of supercooling effects on the sample, and for the purpose of this investigation, the I−N transition was investigated as a function of cooling rate in order to determine the I−N transition temperature at zero cooling rate (T^{o}_{IN}). The effect of the thermal history on the rheological behavior of PSHQ10, in the nematic phase, has been investigated and is reported elsewhere.[56−58]

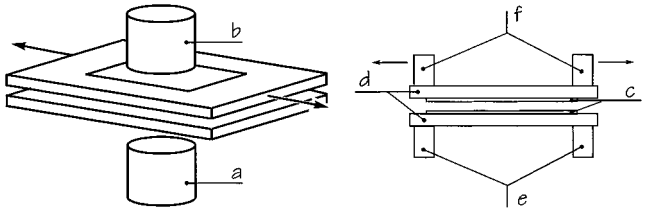

Figure 1. Schematic representation of the rheo-optical experiment employed for microstructural observations during shear flow. Condensed light (a) from the microscope light source is passed through the sample and is sheared by translation of the upper bounding surface and subsequently collected for imaging by a long-working distance objective lens (b). The sample is contained between glass bars (c) heated by embedded mica heaters (slotted for optical access) (d). The forces resulting from sample deformation can be determined by a transducer system connected to the stationary bottom plate (e), while the sample thickness and parallel plate flatness are controlled by a kinematic mount (f) that is mechanically in-line with the stepper motor actuation system.

Rheo-Optics. In-situ rheo-optical measurements were performed in transmission mode in a custom-built parallel-glass-plates shear cell, which has been described elsewhere.[54] A schematic diagram of the experimental setup is shown in Figure 1. This device produces shear flow by sliding one plate with respect to the other (simple shear mode) using a stepper motor and enables microscopic observations under cross-polarized microscopy from room temperature to about 340 °C. The temperature control is better than 0.5 °C. The gap separation can be set accurately by micrometers, and the minimum gap achievable is 20 μm (± 5 μm). The instrument is computer-controlled, making it possible to program different shear protocols under well-controlled conditions (steady shear flow, oscillatory shear flow, etc.). For the observations presented here, the gap separation was set to values between 20 and 50 μm. The optical axis of the microscope is oriented along the velocity gradient direction; therefore, the plane that is imaged contains the velocity (horizontal) and vorticity (vertical) axes. Crossed-polarizers are oriented at 45° to the flow direction. Optical observations were performed with a long working distance lens with 25× magnification. Conoscopic small-angle light scattering (SALS) observations were obtained by passing through the sample a narrow beam of filtered white light ($\lambda \approx 530$ nm) polarized 45° to the flow direction and imaged using a Bertrand lens with an analyzer crossed with the polarizer. Depolarized light scattering patterns (H_V configuration) were obtained by transmitting a polarized He−Ne laser beam through the optical slit in the shearing cell, with the polarization oriented in the flow direction, passing the scattered light through an analyzer oriented in the vorticity direction, and imaging the scattered light pattern on a ground glass plate. Micrographs and diffraction patterns were recorded photographically and video recorded using a CCD video camera (Panasonic model KR222). Frame grabbing and image analysis were performed using Global Lab Image software.[59] Transmitted intensity measurements were made by digitizing microscope images (made using white light from a tungsten lamp) from videotape and computing mean intensities using Global Lab Image software. The obtained intensities were then normalized with respect to the transmitted intensity calculated in the same way for the same sample under quiescent conditions.

Rheology. A model R16 Weissenberg rheogoniometer (Sangamo Control, Inc.) in the cone-and-plate configuration (25 mm diameter plate and 4° cone angle) was used. Oscillatory, steady-state, and transient experiments were employed. From the dynamic storage modulus, $G'(\omega)$, and dynamic loss

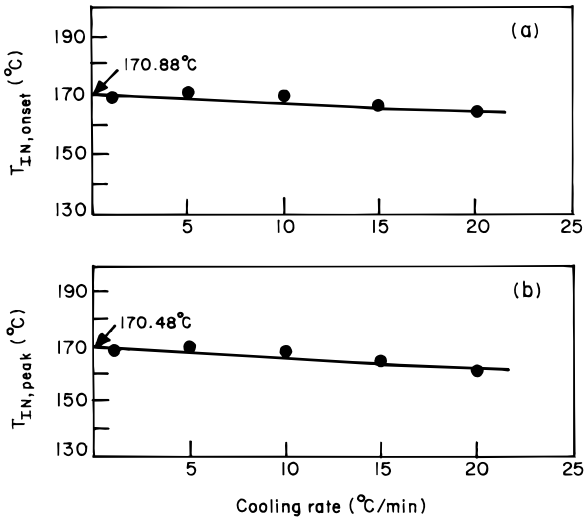

Figure 2. Plots of (a) the onset temperature of the isotropic−nematic (IN) transition ($T_{IN,onset}$) observed during cooling in the DSC versus cooling rate and (b) the peak temperature of the IN transition ($T_{IN,peak}$) versus cooling rate obtained from DSC cooling scans.

modulus, $G''(\omega)$, the complex viscosity $|\eta^*|$ was calculated using the relationship $|\eta^*| = [(G'/\omega)^2 + (G''/\omega)^2]^{1/2}$. Strain amplitude was varied from 0.01 to 0.06, which was well within the linear viscoelastic regime of the material investigated. Data acquisition was accomplished with a microcomputer interfaced to the rheometer. All experiments were conducted under a nitrogen atmosphere to prevent oxidative degradation. The temperature control was accurate to within ±1 °C.

Results and Discussion

Thermal Transitions. The DSC thermogram at 20 °C/min shows that PSHQ10 undergoes a glass transition at ca. 88 °C, a melting of crystals at ca. 115 °C and the nematic−isotropic (N−I) transition at ca. 175 °C.[56] The relevant thermodynamic quantity for the purpose of our investigation is the equilibrium (quiescent) isotropic−nematic (I−N) transition, T^o_{IN}. To determine the value of T_{IN} extrapolated to zero-cooling rate, T^o_{IN}, the following protocol was used. A sample was heated to 200 °C and held isothermally for 3 min to assure thermal equilibrium. Then the sample was cooled past the isotropic−nematic exotherm at varying cooling rates. For each cooling rate investigated, a fresh sample was used. The onset and peak temperatures, respectively, for the observed exotherms were finally plotted versus cooling rate, as shown in Figure 2, and the linear dependence was extrapolated to zero-cooling rate to yield $T^o_{IN,onset} = 170.9$ and $T^o_{IN,peak} = 170.5$ °C. Since the DSC thermogram at the lowest cooling rate employed, 1 °C/min, was observed to be symmetric about the transition temperature, we conclude from Figure 2 that a biphasic window between isotropic and nematic states is only 0.8 °C and is attributed to the polydispersity (ca. 2) of PSHQ10 employed in this study. For simplicity, T^o_{IN} is assigned the value of $T^o_{IN,peak} = 170.5$ °C in further discussions below.

Rheological Properties in the Isotropic Phase. Before attempting an investigation of the effect of shear flow on I−N transition, for future reference we investigated the rheological behavior of PSHQ10 in the isotropic phase. The as-cast PSHQ10 specimen was first heated to a temperature above T^o_{IN} and then subjected to either steady shear or oscillatory shear flow. That the polymer was indeed in the isotropic phase was

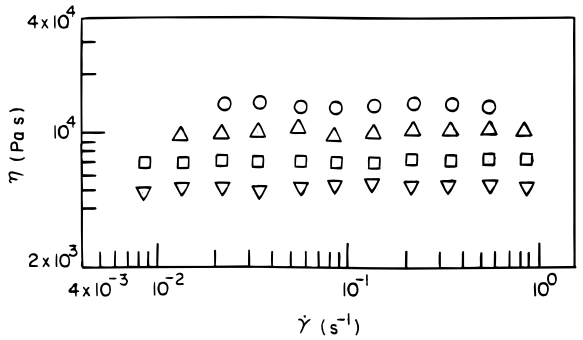

Figure 3. Plots of log η versus log $\dot\gamma$ for PSHQ10 at (○) 180 °C, (△) 185 °C, (□) 191 °C, and (▽) 196 °C.

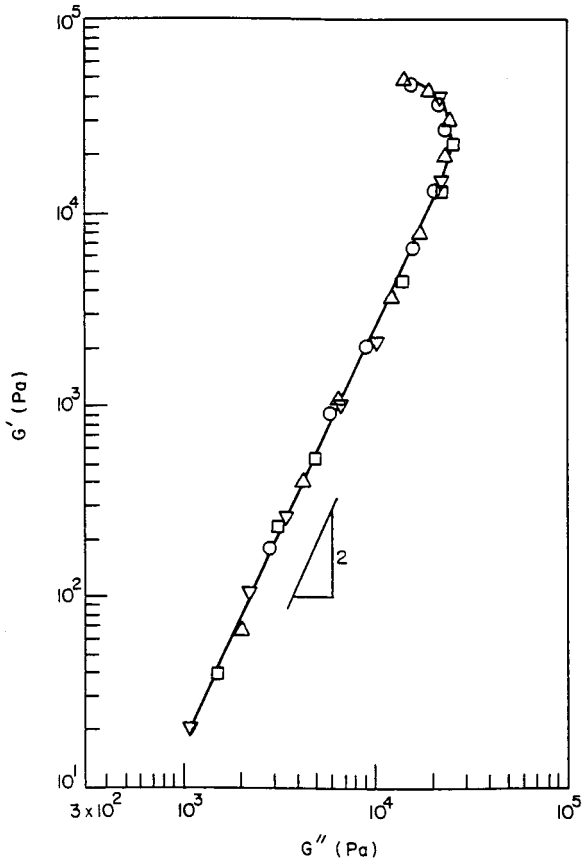

Figure 4. Plots of log G' versus log G'' for PSHQ10 at (○) 180 °C, (△) 185 °C, (□) 191 °C, and (▽) 196 °C.

confirmed via polarized optical microscopy of the same sample at the same temperature. Viewing the sample between crossed polarizers in a transmitted-light microscope, the isotropic phase appears completely black (total extinction) for any orientation of the sample relative to the crossed-polarizers. Figure 3 shows logarithmic plots of steady-state shear viscosity (η) versus shear rate ($\dot\gamma$), at temperatures between 180 and 196 °C. We observe that PSHQ10 displays Newtonian behavior at <ca. 0.5 s^{-1}. In addition, over the same temperature range, PSHQ10 displays virtually zero values of first normal stress difference (N_1). With respect to dynamic oscillatory behavior, Figure 4 shows a plot of log G' versus log G'' for the same temperatures as in Figure 3, indicating temperature independence of the rheological material functions and a slope very close to 2 in the terminal region. It has been shown, experimentally[60] and theoretically,[61] that plots of log G' versus log G'' for homogeneous, isotropic polymeric liquids must exhibit temperature independence. The

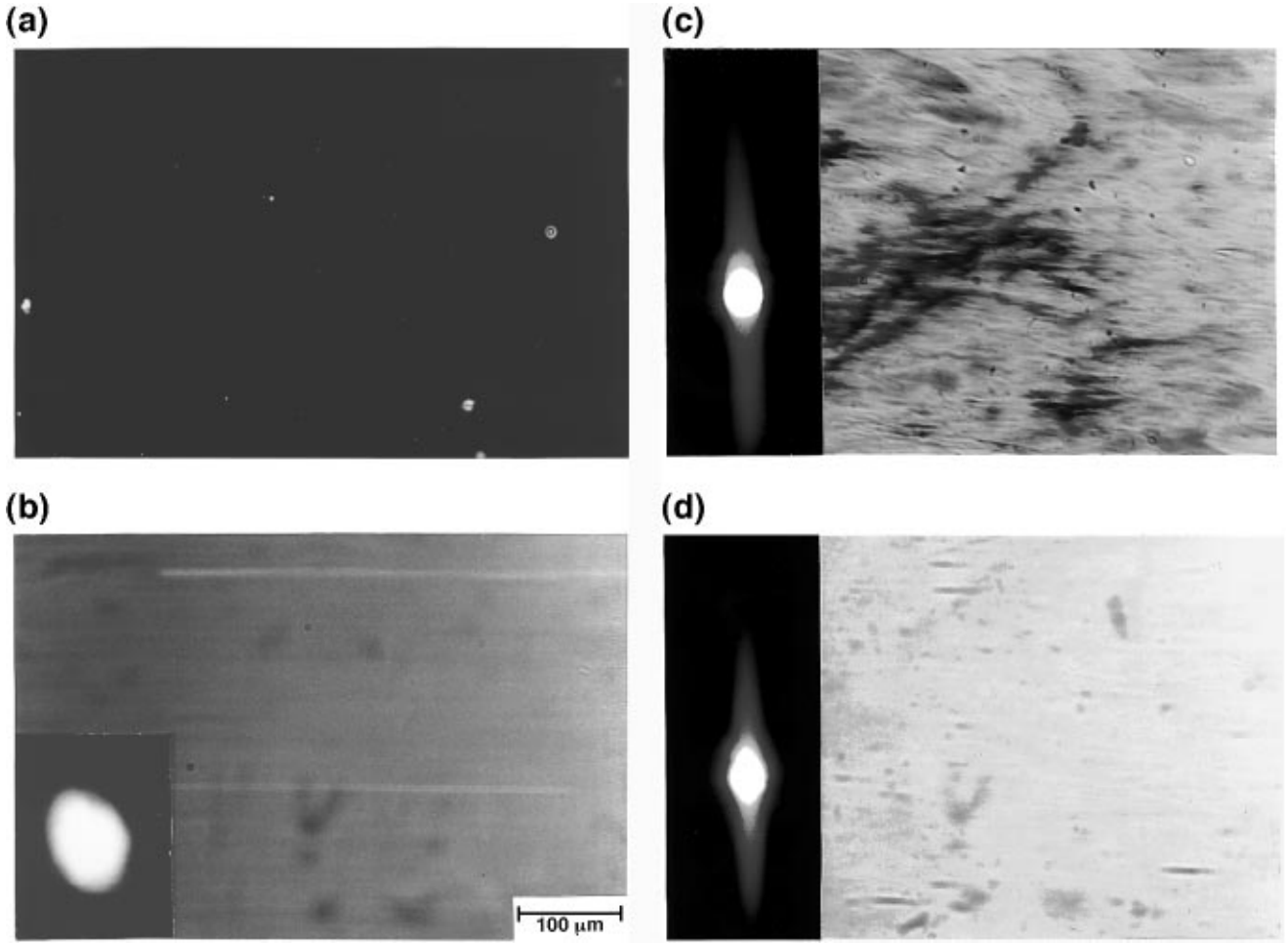

Figure 5. Crossed-polarizer optical micrographs showing the quiescent state (a) prior to flow and (b) during shear flow at $\dot{\gamma} = 0.1\ s^{-1}$ showing slight flow birefringence that quickly disappears after flow cessation. The featureless conoscopic SALS pattern (inset) indicates that no structure is being created in the flow. (c) and (d) are micrographs observed during shearing at $0.8\ s^{-1}$ for accumulated strains of (c) 10 and (d) 50. The temperature is 181 °C, the sample thickness is 20 μm, and the inset bar corresponds to a length of 100 μm. The flow direction is right-to-left, the crossed polarizers are oriented with the polarizer at 45° with respect to the flow, and white light illumination is used.

results in Figures 3 and 4 confirm that PSHQ10 indeed is in the isotropic state over the temperature range investigated. These observations will be useful later on when we relate the rheological properties of PSHQ10 to its morphology in the nematic region.

Flow-Induced I−N Transition. The investigation of the flow-induced I−N transition was conducted in steady shear mode over a range of temperatures above T^{o}_{IN}. For this, a sample was heated to the isotropic phase (ca. 190 °C), held there for 5−10 min, and then cooled slowly to a predetermined temperature, still in the isotropic phase. Steady shear was applied, and the domain texture and shear stress were recorded. We will show that applying shear with increasing $\dot{\gamma}$ leads to a series of structural transitions consistent with flow-induced I−N transition.

When PSHQ10 is sheared at $\dot{\gamma} = 0.1\ s^{-1}$ at 181 °C, it becomes weakly and uniformly birefringent, resulting in an increase in brightness from micrograph a to micrograph b in Figure 5, and consequently, the conoscopic diffraction pattern (shown in inset, Figure 5b) appears featureless because all the structural information is concentrated in the zero-order spot. It is well documented that isotropic polymeric fluids display birefringence ($\Delta n = n_e - n_o \approx 10^{-3}$) in shear flow,[62] and we observe that PSHQ10 demonstrates this behavior under these conditions. It is found, however, that when shear flow is applied with a $\dot{\gamma}$ exceeding a certain critical value, $\dot{\gamma}_c$ (which is found to be temperature dependent), birefringent structures start to nucleate. Micrographs c and d in Figure 5 show the response of PSHQ10 also at 181 °C, but with a larger shear rate, $\dot{\gamma} = 0.8\ s^{-1}$. Initially, the material shows pure flow birefringence. As strain is accumulated, birefringent structures are observed to form, as seen in micrograph c, and these structures assume a fiber-like shape, giving rise to an anisotropic diffraction pattern, shown as the inset to Figure 5c. Increasing the deformation (strain), keeping $\dot{\gamma}$ constant, the fibrils grow in diameter until they start to fill the field of view, as shown in Figure 5d, yielding strong birefringence and transmitted light intensity. While Figure 5d shows a microstructure that is apparently saturated, the micrograph is a snapshot in time of a process that has not reached steady state, as evidenced by continued color changes and transmitted intensity oscillations to strains as high as 250. This time dependence is discussed in detail below in the section on time-evolution of the phase transition.

Interestingly, we also note that the "domains" (fibrils) formed in the isotropic matrix do not show disclinations (discontinuities) in the pattern of molecular alignment but instead are characterized by a uniformly oriented director. This was confirmed by rotating the crossed polarizers parallel and orthogonal to the flow direction.

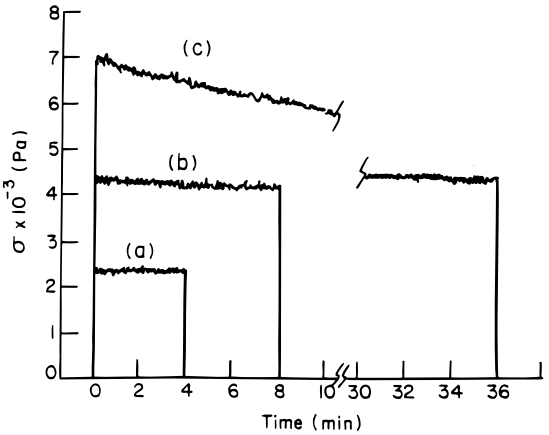

Figure 6. Stress growth traces, $\sigma^+(t,\dot{\gamma})$, for PSHQ10 at 177 °C for various shear rates: (a) 0.14 s^{-1}; (b) 0.27 s^{-1}; (c) 0.43 s^{-1}.

At lower shear rates, but above that required for I−N transition, the fibrils possess dimensions below the limit of our optical resolution (~2 μm) for accumulated strains as large as 300 strain units. Growth of the fibril diameters is therefore dependent on both shear rate *and* the level of accumulated strain.

In a similar manner, the shear stress growth traces change qualitatively in shape as the shear rate is increased. Trace a in Figure 6 shows the shear stress growth ($\sigma^+(t,\dot{\gamma})$) at $\dot{\gamma}$ = 0.14 s^{-1} at 177 °C, conditions yielding simple flow birefringence, as is also the case for the conditions in Figure 5b. We note that $\sigma^+(t,\dot{\gamma})$ reaches a plateau value soon after shear started and remains constant throughout the experiment. After cessation of shear flow, the birefringence and shear stress decay to zero almost immediately, as the material relaxes stress. Increasing the shear rate slightly (e.g., $\dot{\gamma}$ = 0.27 s^{-1}) gives similar optical and rheological results, except that the level of shear stress increases accordingly, as shown by trace b in Figure 6. Above a threshold value of shear rate, the shear stress growth displays a significant overshoot followed by a decay spanning nearly 30 min in time. This long duration decay in the shear stress signal is most likely attributed to the evolution of the biphasic (isotropic + nematic) morphology, as shown in Figure 5c,d. A very similar sequence of stress growth trace shapes is observed at 181 °C, the temperature of the optical observations reported in Figure 5.

The onset for the flow-induced I−N transition at different temperatures was determined independently from relative transmitted intensity (I/I_0) and viscosity (η) measurements by step increases in shear rate. In the case of transmitted intensity measurements, the value obtained upon accumulation of 50 strain units—a value consistent with an apparent steady state—was used for each shear rate, while in the case of viscosity measurements the steady state values were used, irrespective of the strain units accumulated. Figure 7 shows results typical of such experiments which were conducted over a range of temperatures. The shear rate, $\dot{\gamma}$, corresponding to a sudden increase (decrease) in I/I_0 (η) was taken as $\dot{\gamma}_c$ for that temperature. These shear rate values were determined numerically by fitting lines to the shear rate range below and above the knee in the curve at the transition and determining the shear rate corresponding to the intersection of these lines. Transmitted intensity data were obtained using a CCD camera and image analysis processing and were

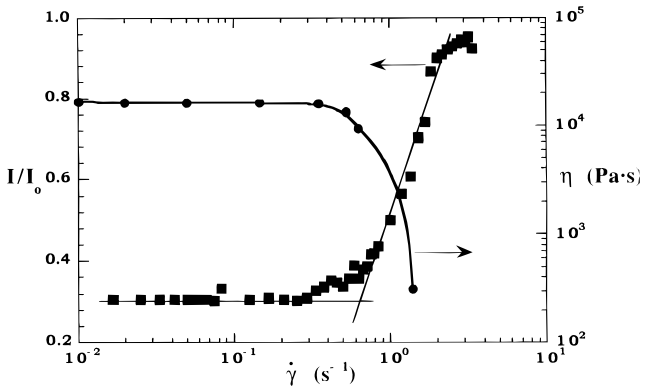

Figure 7. Transmitted light intensity, I/I_0, and steady shear viscosity, η, versus shear rate for T = 180 °C, showing the onset of the flow-induced isotropic−nematic transition above a critical shear rate, $\dot{\gamma}_c$, above which shear viscosity decreases and transmitted intensity increases, each in a critical fashion. Optical measurements were made with the crossed polarizers oriented with the polarizer at 45° with respect to the flow, and white light illumination is used.

normalized relative to the transmitted intensity for crossed polarizers (zero) and parallel polarizers (unity) with identical illumination conditions and no sample present. The increase in I/I_0 corresponds to an increase in the sample birefringence according to the relationship

$$I = I_0 \sin^2\left(2\pi\frac{h\Delta n}{\lambda}\right) \quad (1)$$

as the sample becomes increasingly nematic with accumulated strain. Here, h is the sample thickness, Δn is the birefringence, and λ is the wavelength of incident light.

We note that in gathering viscosity data for determination of the critical shear rate, whenever a sudden drop in viscosity was observed (at a certain $\dot{\gamma}_c$) as $\dot{\gamma}$ was increased, we adopted one of the following two procedures. (a) After shear flow stopped, we monitored the time evolution of $|\eta^*|$ by applying small amplitude oscillatory deformations (at a strain of 0.02 and angular frequency of 0.234 rad/s). When the value of $|\eta^*|$ was determined to show a tendency to level off after a sufficiently long time (say, after 2 h), the specimen was heated to 190 °C and allowed to equilibrate. Then the sample was cooled to the same previous temperature and shear flow was applied again at a higher $\dot{\gamma}$, in accordance with the testing protocol. (b) Another approach adopted was to use a fresh specimen for the next shear flow experiment, and this was chosen whenever we found that the meniscus of the specimen was judged to have been disrupted during the shear flow. It should be emphasized that the strong $\dot{\gamma}$ dependence of viscosity observed in Figure 7 must be distinguished from the so-called "shear-thinning" (or non-Newtonian) behavior of flexible polymers observed for shear rates large enough that $\dot{\gamma}\tau \sim 1$, where τ is the longest relaxation time of the flexible polymer melt.

The optical and rheological determination of the onset of the I−N transition at different temperatures defines a nonequilibrium phase diagram, given in Figure 8, showing that $\dot{\gamma}_c$ increases with increasing $\Delta T = T - T^o_{IN}$, with T being the experimental temperature. This phase diagram defines $\Delta T - \dot{\gamma}_c$ relationships for stabilization of either the isotropic (below the curve) or nematic (above the curve) phase in PSHQ10. The line in Figure 8 corresponds to an exponential fit of the data, yielding the formula: $\dot{\gamma}_c = 0.12e^{0.21\Delta T}$. We note that for

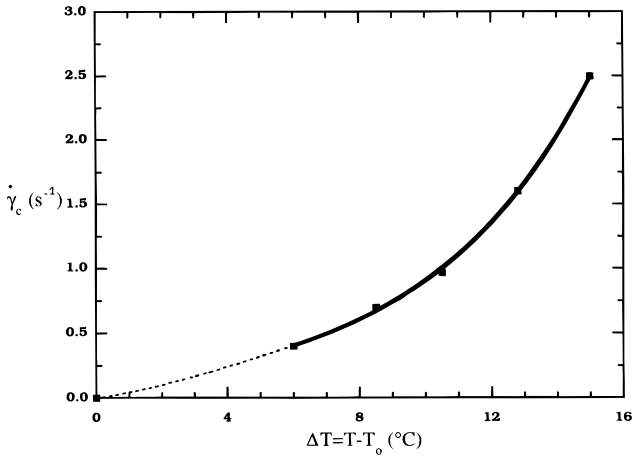

Figure 8. Nonequilibrium phase diagram representing the critical shear rate, $\dot{\gamma}_c$, as a function of temperature, ΔT for the flow-induced isotropic−nematic transition. Each point was determined from the point of rapid rise in the $I/I_0-\dot{\gamma}$ curves and confirmed to within 10% by the onset of dramatic shear thinning observed in $\eta-\dot{\gamma}$ curves.

temperatures sufficiently above T^o_{IN} (e.g., 190 °C) no trace of nematic phase was detected within the range of shear rates explored; i.e., only flow birefringence was produced. It will be shown below that rheological measurements taken before and after prolonged shearing for a range of shear rates showed that, at the same high ΔT values (>15 °C) the viscosity remained constant, indicating that no phase transition could be mechanically detected. The existence of a critical point in this phase diagram, as predicted to exist by Olmsted and Goldbart,[51,52] could not easily be identified.

Time Evolution of the Phase Transition. The time evolution of the isotropic−nematic transition for a number of shear rates satisfying the condition, $\dot{\gamma} > \dot{\gamma}_c$, was examined by measuring *simultaneously* the stress growth trace, transmitted light intensity, and depolarized light scattering patterns as functions of time. In general, it was observed that at lower shear rates, the shear stress and transmitted light intensity rapidly approached their steady-state values and no depolarized light scattering was evident. It should be mentioned that while the stress traces shown were reproducible to within 10%, the level of noise in the data is not unexpected given that the shearing geometry features a sample thickness of 25.4 μm, compared with the usual value of 1.0 mm for most rheological experiments. Figure 9a shows the stress growth and transmitted intensity traces, collected *simultaneously*, for $\dot{\gamma} = 1$ s^{-1} ($\dot{\gamma} > \dot{\gamma}_c$) and $T = 177$ °C ($\Delta T = 6.5$ °C). For this shear rate, the stress trace features a small overshoot at a shear strain of approximately 20 strain units, followed by a slow decay with increasing shear time. The transmitted intensity trace, on the other hand, shows a near linear increase with shearing time, reaching a maximum at a strain near 170 and then decaying and then rising again. Upon cessation of shear flow, the shear stress was observed to decay rapidly.

Figure 9b shows the stress growth and transmitted intensity traces for $\dot{\gamma} = 1.96$ s^{-1}. This shear rate leads to a transmitted intensity curve qualitatively distinct from that observed for $\dot{\gamma} = 1.0$ s^{-1}, as shown in Figure 9a. Here, the transmitted intensity rises rapidly, closely following the stress trace, followed by decay to a pseudosteady value and then by a rise near the end of shearing. The optical response following cessation of shearing becomes increasingly complicated with increasing shear rate, featuring tremendous intensity oscillations and color fluctuations, and will be the subject of further investigation in the future. Also, for $\dot{\gamma} = 1.96$ s^{-1}, small oscillations within the strain range of 50−200 strain units are observed. The amplitude of these intensity oscillations becomes more noticeable at higher shear rates, as is seen in Figure 9c for $\dot{\gamma} = 3.1$ s^{-1} and Figure 9d for $\dot{\gamma} = 3.94$ s^{-1}. For these shear rates, the stress growth trace features a large overshoot and this is accompanied by a large overshoot in transmitted intensity.

Interestingly, strong oscillations in transmitted intensity are observed following the large overshoot in shear stress, as shown in Figure 9c,d. Viewing in the microscope eyepieces during this period of shearing reveals that the intensity oscillations are related to the evolution of the sample birefringence, as evidenced by the passage of a color sequence spanning Newton's color chart in the direction of increasing retardation. [As opposed to oscillations within Newton's color sequence, which would indicate the possibility of thickness oscillations. Additionally, the oscillation in transmitted intensity is not due to thickness variation effects often seen in rotational rheometry of thin samples, as the plates are optically flat and parallel to great precision.] This color sequence is not observed at lower shear rates, $\dot{\gamma} = 1$ s^{-1}, for example, even though they were observed to lead to significant transmitted intensity, indicating $\dot{\gamma} > \dot{\gamma}_c$. More detailed optical investigations are needed to determine, quantitatively, the evolution of birefringence during shear, and these measurements may reveal the origin of changing orientational dynamics with increasing shear rate.

Presented in Figure 10 are digitized photomicrographs corresponding to the points marked "a" through "e" in Figure 9a, which help explain the drop in transmitted intensity observed above a shear strain value of 170. It is seen in Figure 10a−c that the drop in transmitted intensity is related to the coarsening of fibrils such that the intensity within the micrographs becomes less uniform with time, ultimately yielding micrographs that are roughly bimodal in intensity distribution. Because of this, the mean intensity takes on values lower than that corresponding to the peak value of the bright nematic fibrils.

Parts d and e of Figure 10 show, qualitatively, the level of orientation maintained in the sample shortly following cessation of steady shearing, prior to remelting to the equilibrium isotropic phase. Figure 10d, like 10a−c, shows the microstructure in which the sample is viewed between crossed polarizers with the polarizer oriented 45° to the flow axis. It is observed that the sample is quite oriented, leading to significant light transmission. Figure 10e shows the same sample, at nearly the same instant in time, viewed under crossed polarizers with the polarizer oriented in the flow direction. Except for the dust particle imparting birefringence on the nematic in the center of the field of view, nearly no light is transmitted, indicating that the sample is well oriented in the flow direction.

Depolarized light scattering in the H_V configuration is observed for $\dot{\gamma} > \dot{\gamma}_c$. In the H_V configuration, incident light is polarized in the flow direction and the analyzer crossed with the polarizer. The H_V patterns observed during the onset of the flow-induced I−N transition are highly anisotropic with strong scattering in the direction perpendicular to the flow direction, or the vorticity axis. Shown in Figure 11 are the H_V scattering observations

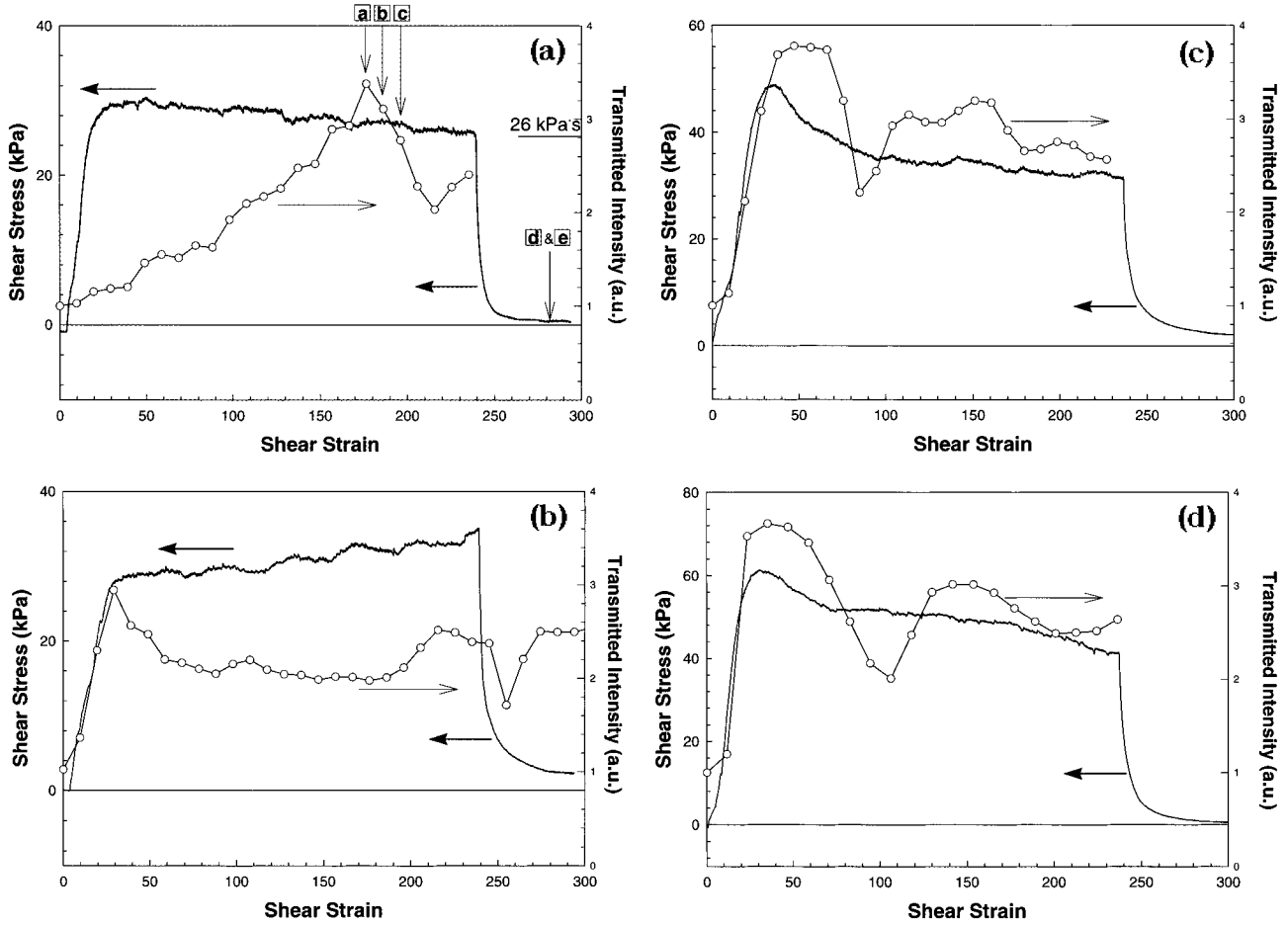

Figure 9. Simultaneous observations of stress growth and transmitted intensity for PSHQ10 sheared for a range of shearing conditions satisfying $\dot{\gamma} > \dot{\gamma}_c$: (a) $\dot{\gamma} = 1.0\ s^{-1}$; (b) $1.96\ s^{-1}$; (c) $3.1\ s^{-1}$; (d) $3.94\ s^{-1}$. $T = 177$ °C, $h = 25.4\ \mu$m. Optical measurements were made with the crossed polarizers oriented with the polarizer at 45° with respect to the flow, and white-light illumination is used.

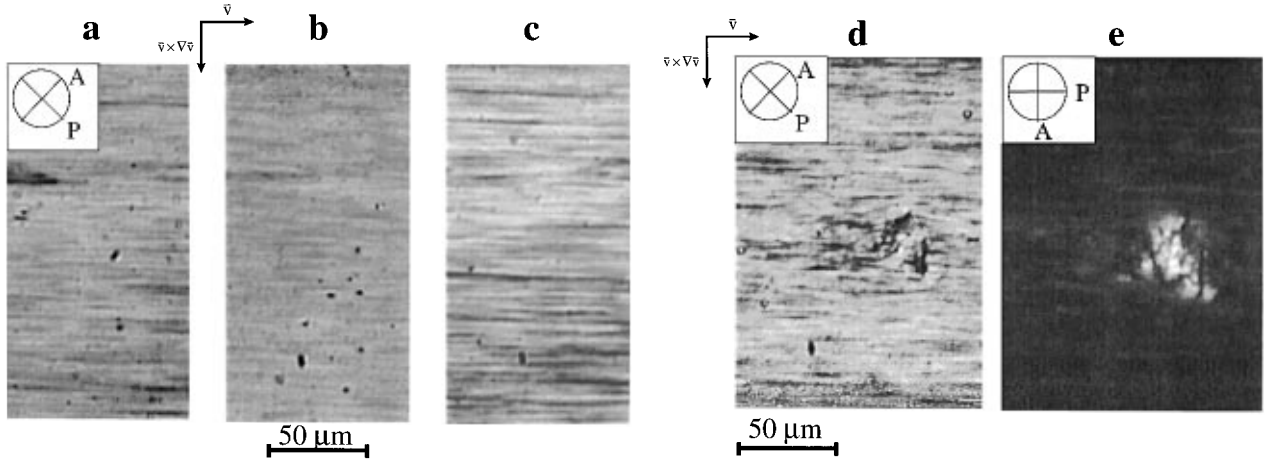

Figure 10. Digitized crossed-polarizer photomicrographs with the polarizer oriented 45° to the flow direction (except (e)) taken at various accumulated strains noted in Figure 9: (a) 176; (b) 186; (c) 196; (d) 282; (e) 282 (polarizer oriented in the flow direction). $T = 177$ °C, $h = 25.4\ \mu$m, and $\dot{\gamma} = 1.0\ s^{-1}$. White-light illumination is used.

for the case $\dot{\gamma} = 1.2\ s^{-1}$ and $T = 177$ °C ($\Delta T = 6.5$ °C), where we plot the intensity profiles along the vorticity axis for accumulated strain values ranging from 2 to 118. Shown as the inset is the full H_V pattern obtained at the accumulated strain value of 50. In this case, and for all other strain values, the level of H_V scattering off of the vorticity axis was negligible. It is found that the *in-situ* H_V scattering observations indicate that the evolution of the nematic−isotropic biphase morphology consists of fibril formation and orientation in the flow direction. Surprisingly, the nematic fibrils (see Figure 5c,d) are apparently regularly spaced in the velocity−vorticity plane, leading to multiple optical diffraction peaks. As strain accumulates, the angle associated with each peak decreases and ultimately all of the peaks shrink to low angles not resolvable with our experimental setup. Therefore, above a strain value of 60, the nematic fibrils appear to coarsen to a diameter substantially larger than the laser wavelength of 632.8 nm. This coarsening of fibril diameters is also accompanied

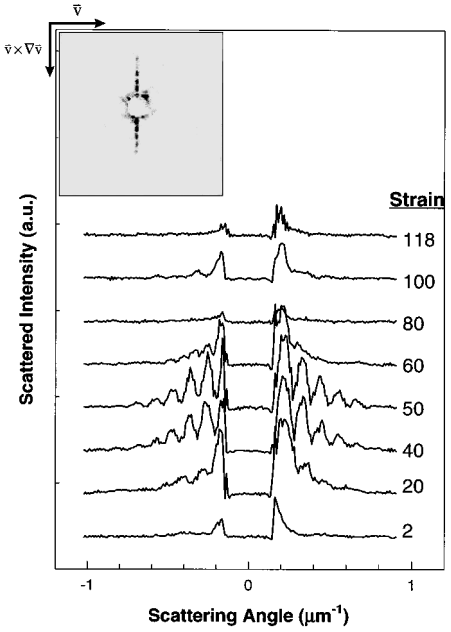

Figure 11. Evolution of anisotropic depolarized (H_V) light scattering patterns observed as intensity profiles along the vorticity axis for $\dot{\gamma} = 1.2\ s^{-1}$ and accumulated strain values: (a) 2; (b) 20; (c) 40; (d) 50; (e) 60; (f) 80; (g) 100; (h) 118. Shown as the inset is the full H_V scattering pattern for $\gamma = 50$. The temperature is 177 °C, and the sample thickness is 25.4 μm. A helium−neon laser is used ($\lambda = 632.9$ nm) with the crossed polarizers oriented with the polarizer oriented parallel to the flow direction. Light is cut off by a beam stop for scattering angles smaller than approximately 0.16 μm^{-1}.

by a scrambling of the regularity in fibril spacing, as is seen from the micrographs in the same strain range for a similar shear rate in Figure 5.

Reversibility of Phase Transition. The flow-induced I−N transition in PSHQ10 is reversible; i.e., the nematic phase that is induced by shear flow "remelts" to a completely isotropic phase over time following shear cessation. Figure 12 gives micrographs taken after cessation of steady shear at 181 °C and 0.8 s^{-1}, in which we observe that upon cessation of shear flow, the birefringent fibrils slowly remelt into the isotropic matrix, as the shear flow stabilizing them is no longer present. It is somewhat surprising that the time required for the remelting of the nematic material takes a much longer time, approximately 30 min for fibrils initially ~5 μm in diameter, when compared to the time required for equilibrium melting of the nematic phase in a hot-stage heating experiment (<1 min). This may be due to a separation of the material by molecular weight during the phase transition such that the core of the nematic fibrils is populated mostly by the macromolecules with the highest molecular weight. In this scenario, the experimental temperature may be lower than the equilibrium nematic−isotropic transition temperature for such a high molecular weight fraction and eventual isotropization will only occur as the molecular weight distribution rehomogenizes by diffusion across the isotropic−nematic interfaces present in the system.

Given the high level of molecular orientation in the nematic fibrils and their large aspect ratio, this diffusion will take place largely in the direction perpendicular to the nematic director. A diffusion coefficient of the magnitude 10^{-11} cm^2/s would be required to explain the slow remelting of flow-induced nematic material based on diffusion-limited kinetics. Tracer diffusion of this

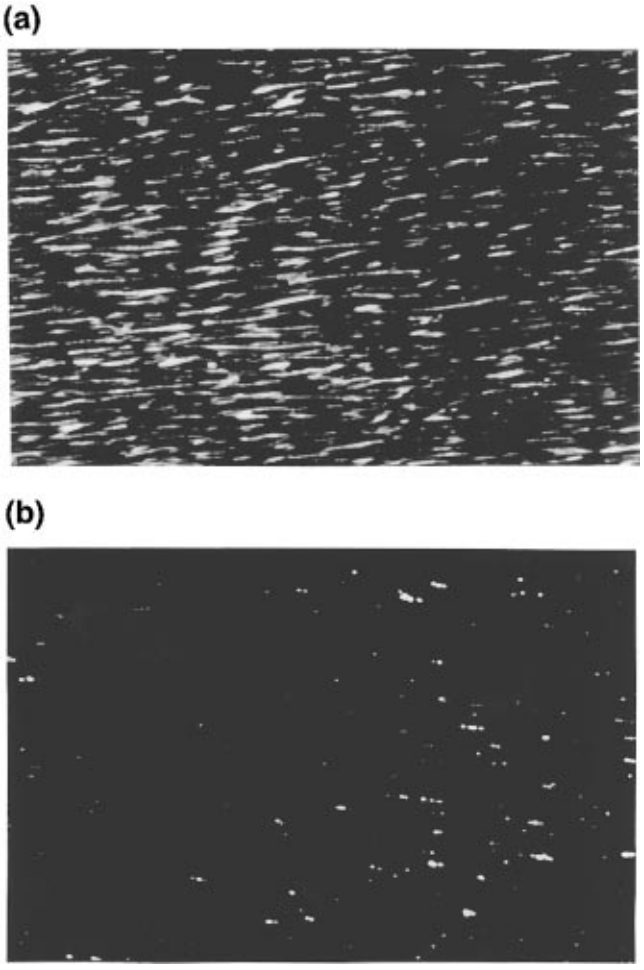

Figure 12. Evolution of the PSHQ10 microstructure following cessation of shear flow for which $\dot{\gamma} = 0.8\ s^{-1} > \dot{\gamma}_c$ where (a) after 5 min the nematic material has significantly melted to a sparse collection of oriented fibrils and (b) 35 min only a small fraction of the sample remains nematic. The temperature is 181 °C, the sample thickness is 25.4 μm, and the micrograph width corresponds to a a length scale of 600 μm. The previous flow direction was left-to-right, and the crossed polarizers are oriented with the polarizer oriented at 45° to the flow direction.

type has been found to yield diffusion coefficients about half the magnitude observed for tracer diffusion, $10^{-12} < D < 10^{-10}$ cm^2/s, just above the nematic−isotropic transition.[63] This diffusion argument is supported by the observation that the time scale for reversal of the I−N transition is longer for increasing durations of shear prior to shear cessation (which yields increasing nematic domain size) and is shown in detail with the rheological measurements discussed below. With increasing domain size resulting from increasing shearing times, the diffusion-limited kinetics leads to longer times for phase-change reversal.

The reversal of the flow-induced I−N transition will necessarily leave its imprint on the rheological properties of the material, given the large difference in the rheological properties of the nematic and isotropic phases of PSHQ10. Therefore, the reversibility to the isotropic phase was examined by small-strain oscillatory measurements where G', G'', and $|\eta^*|$ were monitored before and after shear was applied. Figure 13a shows the evolution of $|\eta^*|$ with rest time t_R at 177 °C after being sheared at 0.43 and 0.68 s^{-1}, respectively, until steady state was reached. The dotted line denotes the value of $|\eta^*|$ just before the sample was subjected to

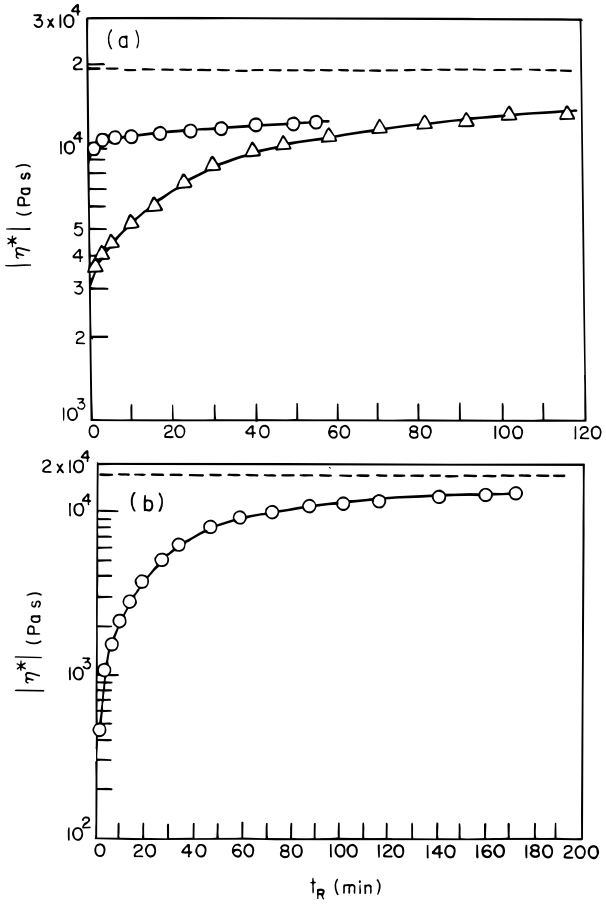

Figure 13. Time evolution of $|\eta^*|$ for the PSHQ10 specimen under small amplitude oscillatory deformations: (a) after the specimen had been subjected to steady shear flow at 177 °C and $\dot{\gamma} = 0.43$ s^{-1} for 36 min (○) and at $\dot{\gamma} = 0.68$ s^{-1} for 57 min (△); (b) after the specimen had been subjected to steady shear flow at 180 °C and $\dot{\gamma} = 1.35$ s^{-1} for 44 min (○). The dotted horizontal line represents the value of $|\eta^*|$ for a specimen before being subjected to steady shear flow.

steady shear flow, and therefore, it represents the melt in the isotropic phase. We note that the value of $|\eta^*|$ increases slowly when the specimen was sheared at 0.43 s^{-1}, as compared to the situation when the sample was sheared at 0.68 s^{-1}, which features a comparatively more rapid increase in $|\eta^*|$ with time. We also note that the higher the $\dot{\gamma}$ value during shear flow, the lower the initial value of $|\eta^*|$ upon cessation of shear flow, and therefore the difference between its initial and final values of $|\eta^*|$ became greater as $\dot{\gamma}$ increased. Figure 13b shows the trend in $|\eta^*|$ with t_R at 180 °C and after shear was applied at 1.35 s^{-1} for 44 min, in which the trend shown in Figure 13a is continued.

Using the dynamic moduli data obtained for Figure 13, we also prepared plots of log G' versus log G'' during the rest period, and they are displayed in Figure 14. Here, the symbol ○ represents the data at 192 °C in the isotropic state that were taken before the specimen had been subjected to shear flow, the symbol ● represents the data taken during the rest period upon cessation of steady shear flow at $\dot{\gamma} = 0.43$ s^{-1} for 36 min, and the symbol ▲ represents data taken during the rest period upon cesssation of steady shear flow at 0.68 s^{-1} for 57 min. It should be mentioned that we used a fixed value (0.238 rad/s) of angular frequency to perform oscillatory shear flow experiments at preset time intervals during the entire rest period. The caption of Figure 14 describes the time, t_R, at which each data point

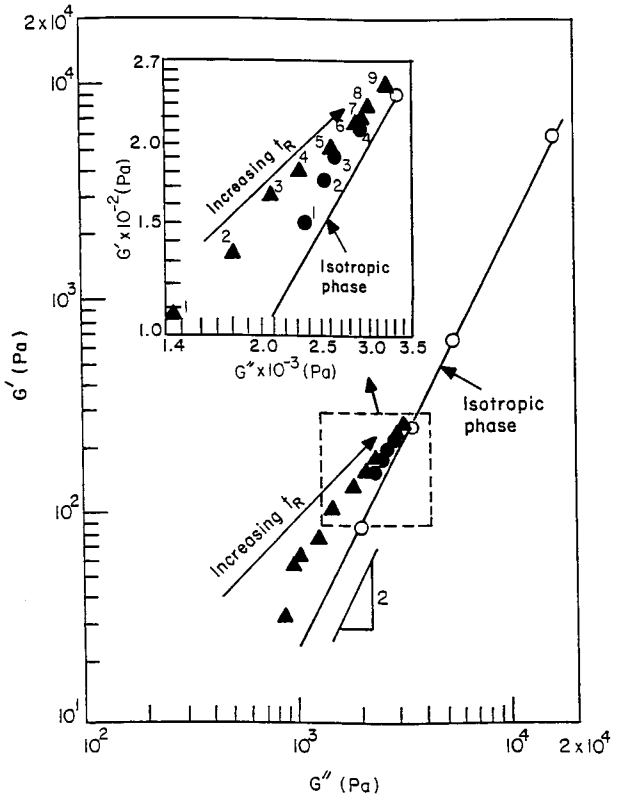

Figure 14. Plots of log G' versus log G'' for a PSHQ10 specimen: (○) at 192 °C; (●) during the rest period (t_R) of 55 min after the specimen at 177 °C had been subjected to steady shear flow at $\dot{\gamma} = 0.43$ s^{-1} for 36 min, where the number next to each symbol identifies the time at which the particular oscillatory shear flow experiment at an angular frequency of 0.238 rad/s was conducted [(1) $t_R = 1$ min; (2) $t_R = 3$ min; (3) $t_R = 10$ min; (4) $t_R = 48$ min]; (▲) during the rest period (t_R) of 155 min after the specimen at 177 °C had been subjected to steady shear flow at $\dot{\gamma} = 0.68$ s^{-1} for 57 min, where the number next to each symbol identifies the time at which the particular oscillatory shear flow experiment at an angular frequency of 0.238 rad/s was conducted [(1) $t_R = 1$ min; (2) $t_R = 5$ min; (3) $t_R = 16$ min; (4) $t_R = 30$ min; (5) $t_R = 39$ min; (6) $t_R = 58$ min; (7) $t_R = 71$ min; (8) $t_R = 82$ min; (9) $t_R = 116$ min].

(indicated by a number next to each symbol) was taken during the rest period. It can be seen from Figure 14 that the deviation from the log G' versus log G'' plots corresponding to the isotropic state (○) increases as the shear rate prior to cessation increases from 0.43 s^{-1} (●) to 0.68 s^{-1} (▲). We thus conclude not only that the specimen had been driven to a nematic state but also that soon after shear cessation the nematic state of the specimen was rheologically more distinct from the isotropic state as the previous shear rate increased.

We wish to point out that we do not attach any significance to the slope of log G' versus log G'' plots obtained during the rest period upon cessation of shear flow. What is significant in Figure 14 is the direction in which the data points (● or ▲) move as t_R increases. Specifically, the late time data points for both postflow data sets approach very closely the data point (symbol ○ shown in the inset plot of Figure 14) taken at 192 °C in the isotropic state at an angular frequency of 0.238 rad/s, which is the same value as that employed in oscillatory shear flow experiments during the rest period following shear cessation.

It seems appropriate to mention at this juncture that, earlier, a reversed phase transition was also reported by Silverberg and Kuhn[8] who observed shear-induced

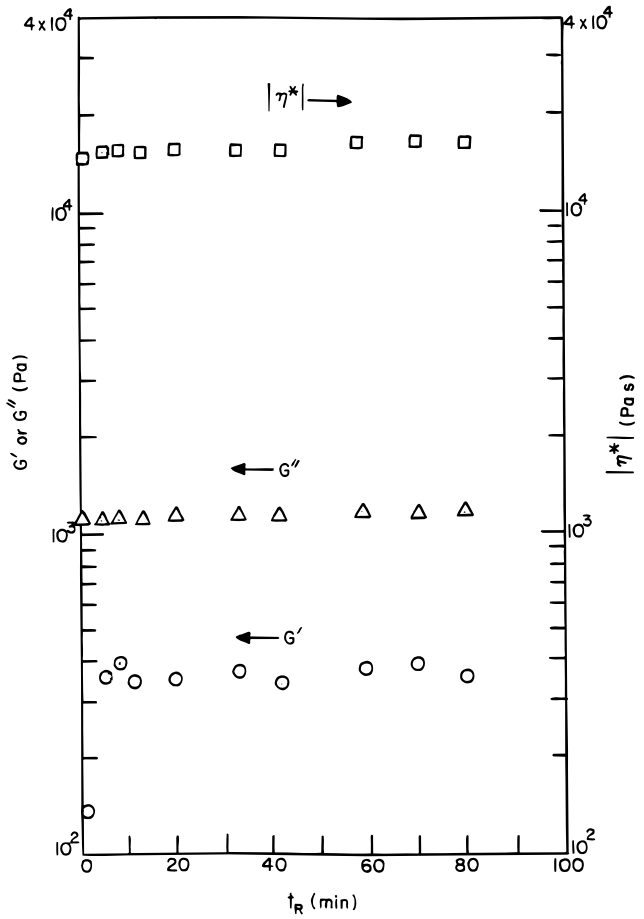

Figure 15. Plots of G', G'', and $|\eta^*|$ for a PSHQ10 specimen at 130 °C under small amplitude deformations after the specimen had been subjected to steady shear flow at $\dot{\gamma} = 0.11$ s^{-1} for 22 min.

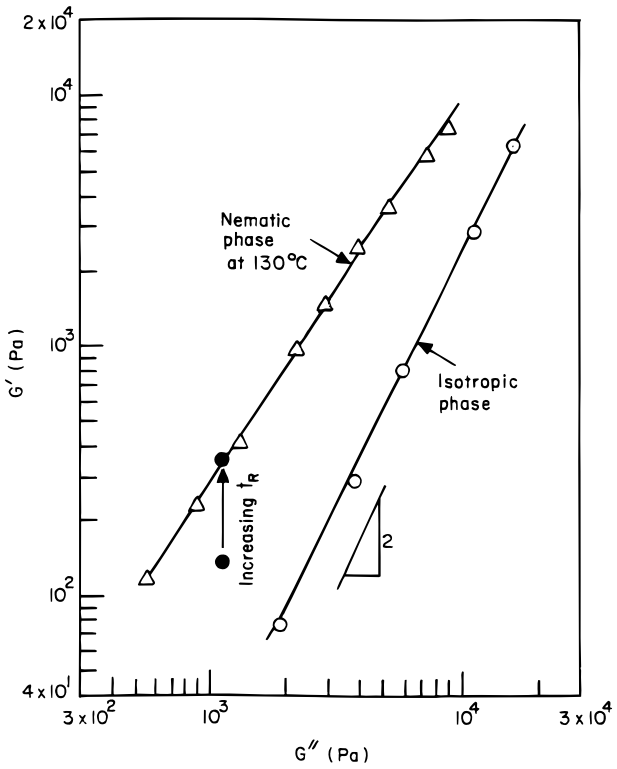

Figure 16. Plots of log G' versus log G'' for a PSHQ10 specimen: (○) at 192 °C; (●) during the rest period of 80 min after the specimen had been subjected to steady shear flow at $\dot{\gamma} = 0.11$ s^{-1} for 22 min at 130 °C; (△) at the end of the rest period of 80 min after the specimen had been subjected to steady shear flow at $\dot{\gamma} = 0.11$ s^{-1} for 22 min at 130 °C.

mixing of a two-phase liquid mixture, and by Ver Strate and Philippoff[3] who reported shear-induced phase separation in a dilute polymer solution.

Rheology in the Nematic State. At this point it would be important to present data concerning the rheological behavior of PSHQ10 in the nematic state after being sheared, and observe the time evolution of G' and G''. For this, we employed the following experimental protocol: (a) an as-cast specimen was first heated to 192 °C, and after thermal equilibration, the specimen was sheared at 0.008 s^{-1} for 4 min; (b) oscillatory shear flow was applied at several angular frequencies (ω) from which log G' versus log G'' plots were obtained; (c) the specimen was cooled very slowly to 130 °C over a period of 90 min. After thermal equilibration, the specimen was sheared at 0.11 s^{-1} for 22 min, and (d) after cessation of shear flow, small amplitude oscillatory shear flow at $\omega = 0.075$ rad/s with a strain of 0.02 was applied to the specimen to monitor the time evolution of G' and G''.

Figure 15 shows the time evolution of G' and G'', and $|\eta^*|$ after cessation of steady shear flow at 0.11 s^{-1} and 130 °C. It can be seen in Figure 15 that within 2 min after cessation of shear flow G' increased rapidly and then remained more or less constant for a period of 75 min, while both G'' and $|\eta^*|$ remained more or less constant for the entire period of 80 min after cessation of shear flow. In view of the fact that the magnitude of G' is much smaller than that of G'', the value of $|\eta^*|$ is predominantly determined by the magnitude of G''. Notice that the time evolution of $|\eta^*|$ after cessation of steady shear flow given in Figure 15 is quite different from that given in Figure 13. The difference between the two situations is that at $T = 130$ °C, far away from the T_{NI} of PSHQ10 ($\Delta T = -40$ °C), there is no chance of phase reversal, after cessation of steady shear flow, moving from the nematic state to the isotropic state. Therefore, in Figure 15 we observe more or less constant values of G', G'', and $|\eta^*|$ during the rest period of 100 min, suggesting that the morphology of the specimen remained constant during the same period. It should be remembered that in Figure 13 we observed a phase reversal, upon cessation of steady shear flow, taking place when a PSHQ10 specimen was driven from the isotropic state by an applied shear flow.

Figure 16 gives a log G' versus log G'' plot at 130 °C (●), in which we observe that the value of G', after cessation of shear flow, moved rapidly upward and then remained stable during the rest period of 75 min. This observation supports our view that the morphology of the specimen remained unchanged during the same period. After the total rest period of 80 min the specimen was subjected to oscillatory shear flow over a range of ω, and the results are also plotted in Figure 16 (△). For comparison, plots of log G' and log G'' at 192 °C in the isotropic state are also included in Figure 16 (○). Note that the data obtained after PSHQ10 was sheared at 130 °C remained on the left side of the corresponding plot in the isotropic state. Han et al.[64–66] have shown that log G' versus log G'' plots are virtually independent of temperature, giving rise to a slope of 2 in the terminal region, for block copolymers in the disordered (homogeneous) state (i.e., at temperatures above the order-disorder transition temperature, T_{ODT}), and they become dependent upon temperature in the

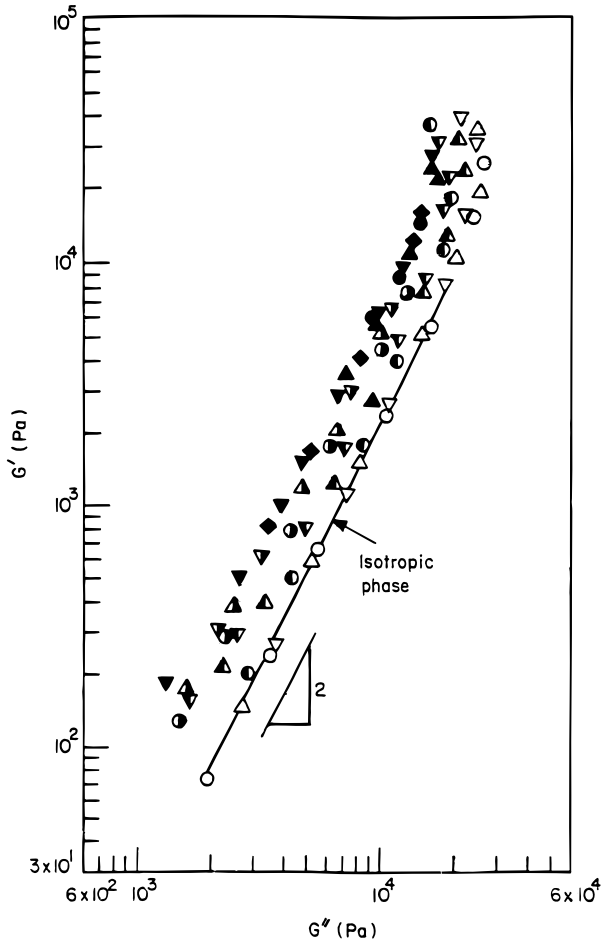

Figure 17. Plots of log G' versus log G'' for a PSHQ10 specimen at various temperatures: (○) 192 °C; (△) 185 °C; (▽) 180 °C; (◐) 175 °C; (▲) 173 °C; (▼) 170 °C; (◑) 163 °C; (◭) 160 °C; (▼) 154 °C; (◆) 144 °C; (▼) 140 °C; (▲) 135 °C; (●) 130 °C.

ordered state (i.e., at $T < T_{ODT}$), lying on the left side of the log G' versus log G'' for the disordered state. Moreover, as the temperature increased toward the T_{ODT} of a block copolymer, its log G' versus log G'' plot approached that in the disordered state. Indeed, we observe a similar trend for PSHQ10, as shown in Figure 17. Note that the experimental results summarized in Figure 17 were obtained by taking oscillatory shear flow measurements, without prior shear flow, under isothermal conditions. These results demonstrate that log G' versus log G'' plots are very sensitive to the morphological state of PSHQ10, and potentially of TLCPs in general. It should be mentioned that Figure 17 was obtained by placing a specimen into the cone-and-plate fixture of the rheometer, which was preheated to 192 °C in the isotropic state. After thermal equilibration, a dynamic frequency sweep experiment was conducted first at 192 °C, in the isotropic state far above T^o_{IN}. Then, the temperature of the specimen was lowered slowly, stepwise, to a preset temperature in the nematic state, which lasted ca. 20 min at each temperature interval chosen, and a dynamic frequency sweep experiment was conducted under isothermal conditions for angular frequencies spanning 0.15−7.5 rad/s.

Concluding Remarks

In this paper we have presented experimental confirmation of flow-induced I−N transition in a TLCP, PSHQ10. Using a novel rheo-optical technique, we found that the farther away the experimental temperature of a specimen from its T^o_{IN}, the larger the value of $\dot{\gamma}_c$. We have shown that a sudden drop in η at $\dot{\gamma} > \dot{\gamma}_c$ is accompanied by the formation of birefringent oriented fibrils in the otherwise isotropic matrix, proving that the I−N transition is occurring during shear flow. By varying temperature and $\dot{\gamma}$, a nonequilibrium phase diagram has been constructed. It is also shown that the I−N transition is associated with a kinetic process in that the duration of shear affects the extent of the phase transition and a reversed phase transition takes place after cessation of shear flow. That the nematic mesophase is aligned along the flow direction, thus giving rise to viscosities lower than those in the isotropic phase, has a practical significance in the processing of TLCPs; i.e., their viscosities can be kept low (and thus the throughput can be increased) by being able to maintain the liquid-crystalline state at higher $\dot{\gamma}$.

The experiments reported here show that the initially disordered, semiflexible TLCP, PSHQ10, in the isotropic phase tends to align along the flow direction under the influence of shear flow, giving rise to an orientational (nematic) correlation of the molecular chains and therefore to a flow-induced I−N transition. Similar experiments on other TLCPs[23] showed that the apparent N−I phase boundary shifts to higher temperatures with increasing $\dot{\gamma}$, indicating that in a shear field the chains persist in their extended conformation at $T > T^o_{IN}$. The suggestion that shear flow can alter the temperature dependence of the LCP persistence length seems very reasonable, although to our knowledge it has not been examined in detail.

We believe that the I−N transition is a continuous process, where the accumulation of strain transforms the isotropic phase to a nematic phase. It has been shown that in a biphasic region the higher molecular weight component of a polydisperse liquid-crystalline polymer is the one contributing to the nematic phase.[67] Along this line, the phase reversal observed in PSHQ10 corresponds to the remelting, first of its lower molecular weight component, followed by its higher molecular weight component; i.e., there is a molecular weight selection in the phase reversing process.

The flow-induced I−N transition reported in this study is important from a practical viewpoint in that it can eliminate any deleterious impact of a disordered phase, for instance, in the melt spinning process. A case in point is the formation of banded texture, consisting of approximately equidistant extinction bands (as observed between crossed polarizers) running perpendicular to the flow direction.[68] Banded texture is believed to result from the relaxation of stored distortional (curvature) elasticity and is an optical manifestation of a misalignment of the preferred direction of molecular orientation relative to the shear direction, with the degree of misalignment varying periodically as a function of position measured along the shear direction. It can be surmised that the presence of banded texture is detrimental to the modulus, for instance, of extruded products along the shear direction,[69,70] because loads applied in this direction can stretch the not-so-fully aligned mesophase. Thus the banded texture can be regarded as being a processing defect in TLCPs. Shown in Figure 18 is a direct comparison of microstructures resulting from two different thermomechanical histories. **Case I:** Shear flow is applied to PSHQ10 at a temperature $T > T^o_{IN}$ with a shear rate $\dot{\gamma} > \dot{\gamma}_c$. After

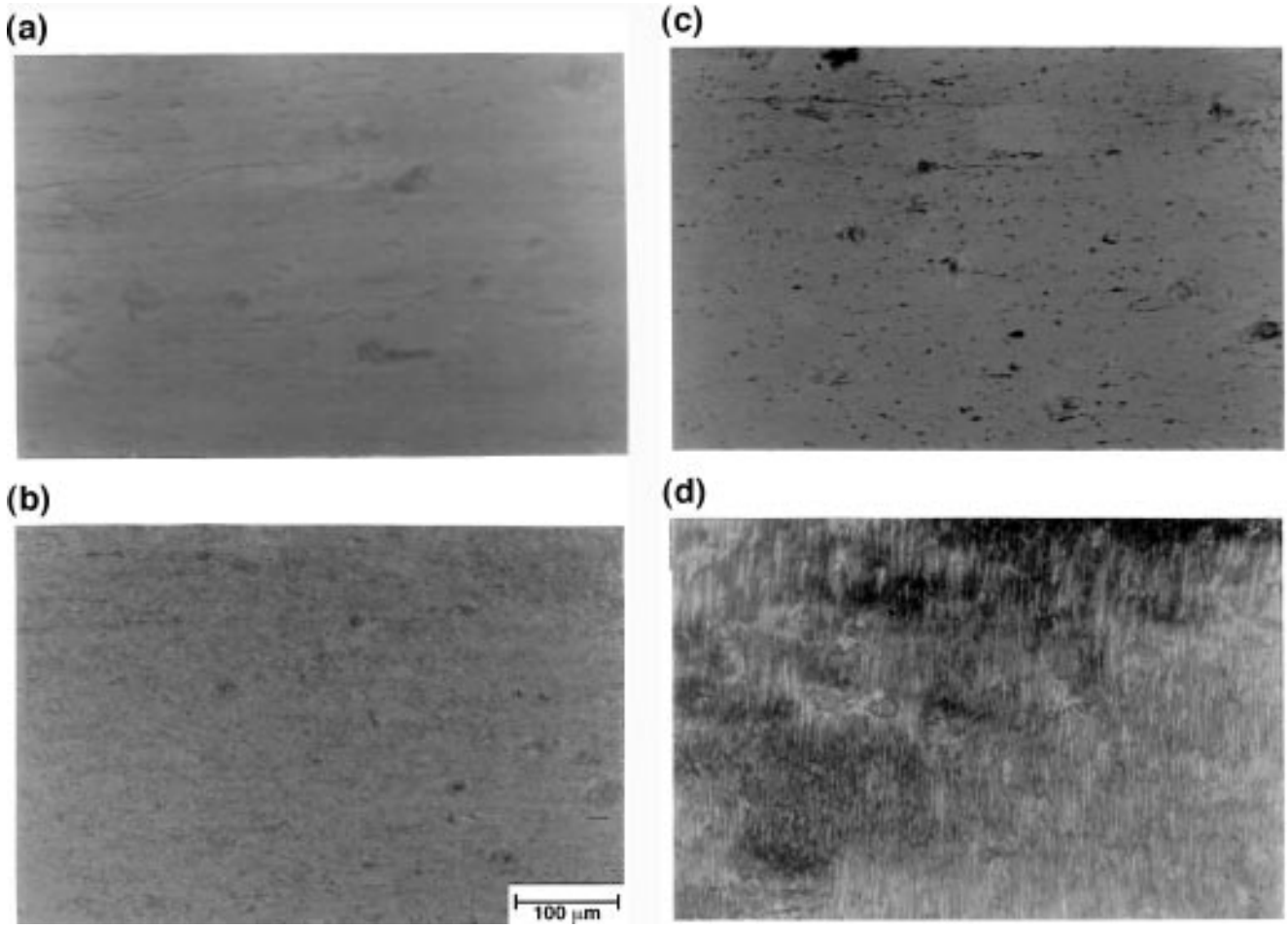

Figure 18. Thermotropic PSHQ10 at $T = 181$ °C ($\Delta T = 10.5$ °C) was sheared at $\dot{\gamma} = 1.0$ s^{-1} ($>\dot{\gamma}_c$), in order to induce the I−N transition, and then cooled to the liquid crystalline (LC) phase ($\Delta T = -10.5$ °C) at 5 °C/min with shearing. Once in the nematic phase, the shear was stopped. Optical micrographs with crossed polarizers oriented with the polarizer at 45° to the flow direction were taken (a) 1 min and (b) 30 min following cessation of shear. The experiment was repeated at the same shear rate, but this time solely in the nematic phase ($\Delta T = -10.5$ °C). Micrographs were taken (c) 1 min and (d) 5 min following cessation of shear. Green-filtered incident light was used resulting in lower intensity micrographs.

shearing 100 strain units, having induced a significant level of nematic ordering, the temperature was gradually reduced to $T = 160$ °C ($\Delta T = -10.5$ °C) with shearing. This protocol leads to uniform birefringence that is stable after flow is removed, as shown in Figure 18a, 1 min after flow, and Figure 18b, taken 30 min after flow. We note that the glass surfaces have not been treated to align the nematic director in any preferred direction, so that it is fully expected that at long times the director field will become disoriented in accord with incommensurate orientational boundary conditions. **Case II:** Shear flow of the same shear rate and the same total strain units as in case I is applied at $T = 160$ °C. Following flow cessation, the high level of orientation, as indicated in Figure 18c, 1 min post-shear, is quickly destroyed by the onset of bands perpendicular to the flow direction, as shown in Figure 18d.

This somewhat surprising dependence of the relaxed microstructure on the thermomechanical history suggests that the materials shown in Figure 18a,c, while appearing quite similar in their significant degree of shear-induced alignment, are actually quite different in their level of disclination content. The fact that the microstructure seen in Figure 18c relaxes to a defect-ridden banded texture shows that during shear the orientational defects, or disclinations, are not removed by the shearing flow that tends to align the nematic director but are instead compressed under the competition of viscous to elastic stresses, to a dimension smaller than that discernible with our magnification. In contrast, the I−N transition offers two possible mechanisms for the production of a relatively defect-free nematic director, at least one of which is apparently in effect, as seen in Figure 18b. One possibility is that the growth of the nematic phase is nucleated from a collection of extended chains that naturally leads to nematic regions which are free from disclinations, as in the case of surface orientation of nematics. Should disclinations form during the growth of fibrils, however, it is conceivable they can be removed by director unwinding at the nematic−isotropic interface. According to Meyer,[71] disclinations within a characteristic length of an interface, $\alpha_D = K/\sigma_A$, will be attracted to the interface and annihilated through director reorientation if the alignment boundary condition is sufficiently weak. Here, K is a Frank elastic constant, and σ_A is the anisotropy in surface tension for the director perpendicular to the interface versus parallel to the interface. The rather long orientational relaxation time associated with the flow-induced nematic mesophase opens up the possibility of new processing routes for defect-free TLCPs.

Acknowledgment. A.R-U and P.T.M. acknowledge the financial support of the U.S. Air Force Office of

Scientific Research (AFOSR), the USAF Phillips Laboratory Propulsion Directorate, and the USAF Wright Laboratory Materials Directorate. P.T.M. acknowledges enlightening discussions with Prof. Steven Hudson pertaining to defect removal at interfaces.

References and Notes

(1) Miller, R. L., Ed. *Flow-induced Crystallization in Polymer Systems*; Gordon and Breach: New York, 1979.
(2) McHugh, A. J.; Blank, R. H. *Macromolecules* **1986**, *19*, 1187.
(3) Ver Strate, G.; Philippoff, W. *J. Polym. Sci., Polym. Lett. Ed.* **1974**, *12*, 267.
(4) Rangel-Nafaile, C.; Metzner, A. B.; Wissbrun, K. *Macromolecules* **1984**, *17*, 1187.
(5) Hammouda, B.; Nakatani, A. I.; Waldow, D. A.; Han, C. C. *Macromolecules* **1992**, *25*, 2903.
(6) Onuki, A. *Phys. Rev. Lett.* **1989**, *62*, 2472.
(7) Larson, R. G. *Rheol. Acta* **1992**, *31*, 497.
(8) Silverberg, A.; Khun, W. *J. Polym. Sci.* **1954**, *13*, 21.
(9) Mazich, K. A.; Carr, S. H. *J. Appl. Phys.* **1983**, *54*, 5511.
(10) Katsaros, J. D.; Malone, M. F.; Winter, H. H. *Polym. Bull.* **1986**, *16*, 83.
(11) Lyngaae-Jorgensen, J.; Sondergaard, K. *Polym. Eng. Sci.* **1987**, *27*, 344.
(12) Hindawi, I.; Higgins, J. S.; Galambos, A. F.; Weiss, R. A. *Macromolecules* **1990**, *23*, 670.
(13) Donald, A. M.; Windle, A. H. *Liquid Crystalline Polymers*; Cambridge University Press: Cambridge, U.K., 1992.
(14) Collyer, A. A., Ed. *Liquid Crystal Polymers: from Structures to Applications*; Elsevier Applied Science: London, 1992.
(15) Graziano, D. J.; Mackley, M. R. *Mol. Cryst. Liq. Cryst.* **1984**, *106*, 73.
(16) Picken, S. J.; Aerts, J.; Visser, R.; Northolt, M. G. *Macromolecules* **1990**, *23*, 3849.
(17) Odell, J. A.; Ungar, G.; Feijoo, J. L. *J. Polym. Sci., Polym. Phys.* **1993**, *31*, 141.
(18) Gervat, L.; Mackley, M. R.; Nicholson, T. M.; Windle, A. H. *Phil. Trans. R. Soc. London* **1995**, *A350*, 1.
(19) Hanna, S.; Romo-Uribe, A.; Windle, A. H. *Nature* **1993**, *366*, 546.
(20) Romo-Uribe, A.; Windle, A. H. *Macromolecules* **1993**, *26*, 7100.
(21) Romo-Uribe, A.; Windle, A. H. *Macromolecules* **1996**, *29*, 6246.
(22) Wissbrun, K. F.; Griffin, A. C. *J. Polym. Sci., Polym. Phys. Ed.* **1982**, *20*, 1835.
(23) Wunder, S. L.; Ramachandran, S.; Gochanour, C. R.; Weinberg, M. *Macromolecules* **1986**, *19*, 1696.
(24) Irwin, R. S.; Sweeny, W.; Gardner, K. H.; Gochanour, C. R.; Weinberg, M. *Macromolecules* **1986**, *19*, 1696.
(25) Driscoll, P.; Masuda, T.; Fujiwara, K. *Macromolecules* **1991**, *24*, 1567.
(26) Romo-Uribe, A.; Lemmon, T.; Windle, A. H. *J. Rheol.* **1997**, *41*, 1117.
(27) (a) Kim, S. S.; Han, C. D. *Macromolecules* **1993**, *26*, 6633. (b) Kim, S. S.; Han, C. D. *J. Rheol.* **1993**, *37*, 847. (c) Kim, S. S.; Han, C. D. *J. Polym. Sci., Part B: Polym. Phys.* **1994**, *32*, 371.
(28) Han, C. D.; Kim, S. S. *J. Rheol.* **1994**, *38*, 13. (b) Han, C. D.; Chang, S. *J. Rheol.* **1994**, *38*, 241.
(29) Han, C. D.; Chang, S.; Kim, S. S. *Mol. Cryst. Liq. Cryst.* **1994**, *254*, 335.
(30) Baek, S.-G.; Magda, J. J.; Larson, R. G.; Hudson, S. D. *J. Rheol.* **1994**, *38*, 1473.
(31) Gilmore, J. R.; Colby, R. H.; Hall, E.; Ober, C. K. *J. Rheol.* **1994**, *38*, 1623.
(32) (a) Kiss, G.; Porter, R. S. *J. Polym. Sci., Polym. Symp.* **1978**, *65*, 193. (b) Kiss, G.; Porter, R. S. *J. Polym. Sci., Polym. Phys.* **1980**, *18*, 361. (c) Kiss, G.; Porter, R. S. *Mol. Cryst. Liq. Cryst.* **1980**, *60*, 267.
(33) Chu, G.; Venkatraman, S.; Berry, G. C.; Einaga, Y. *Macromolecules* **1981**, *14*, 939.
(34) Navard, P.; Haudin, J. M. *J. Polym. Sci., Polym. Phys.* **1986**, *24*, 189.
(35) Einaga, Y.; Berry, G. C.; Chu, S. G. *Polym. J.* **1985**, *17*, 239.
(36) Mead. D. W.; Larson, R. G. *Macromolecules* **1990,** *23*, 2524.
(37) Chow, A. W.; Fuller, G. G. *Macromolecules* **1985**, *18*, 786.
(38) Doppert, H. L.; Picken, S. J. *Mol. Cryst. Liq. Cryst.* **1987**, *153*, 109.
(39) Chow, A. W.; Hamlin, R.; Ylitalo, C. M. *Macromolecules* **1992**, *25*, 7135.
(40) Grizzuti, N.; Cavella, S.; Cicarelli, P. *J. Rheol.* **1990**, *30*, 1293.
(41) (a) Moldenaers, P.; Mewis, J. *J. Rheol.* **1986**, *30*, 567. (b) Moldenaers, P.; Yanase, H.; Mewis, J. *J. Rheol.* **1991**, *35*, 1681. (c) Moldenaers, P.; Mewis, J. *J. Rheol.* **1993**, *37*, 367.
(42) (a) Baek, S. G.; Magda, J.; Larson, R. G.; Hudson, S. D. *J. Rheol.* **1993**, *37*, 1201. (b) Baek, S. G.; Magda, J. J.; Cementwala, S. *J. Rheol.* **1993**, *78*, 935.
(43) (a) MacDonald, W. A.; McLenaghan, A. D. W.; McLean, G.; Richards, R. W.; King, S. M. *Macromolecules* **1991**, *24*, 6164. (b) Muhlebach, A.; Economy, J.; Johnson, R. D.; Karis, T.; Lyerla, J. *Macromolecules* **1990**, *23*, 1803. (c) Jin, J.-I.; Chang, J.-H.; Hatada, K.; Ute, K.; Hotta, M. *Polymer* **1992**, *33*, 1374.
(44) Ambrose, E. J. *Symp. Faraday Soc.* **1971**, *5*, 175.
(45) Kerkam, K.; Viney, C.; Kaplan, D.; Lombardi, S. *Nature* **1991**, *349*, 596.
(46) Marrucci, G.; Ciferri, A. *J. Polym. Sci., Polym. Lett. Ed.* **1977**, *15*, 643.
(47) Flory, P. J. *Proc. R. Soc. London* **1956**, *A234*, 73.
(48) Thirumalai, D. *J. Chem. Phys.* **1986**, *84*, 5869.
(49) See, H.; Doi, M.; Larson, R. G. *J. Chem. Phys.* **1990**, *92*, 792.
(50) Han, C. D.; Kim, S. S. *Macromolecules* **1995**, *28*, 2089.
(51) Olmsted, P. D.; Goldbart P. M. *Phys. Rev. A* **1990**, *41*, 4578.
(52) Olmsted, P. D.; Goldbart P. M. *Phys. Rev. A* **1992**, *46*, 4966.
(53) Safinya, C. R.; Sirota, E. B.; Plano, R. J. *Phys. Rev. Lett.* **1991**, *66*, 1986.
(54) Mather, P. T.; Stüber, H. R.; Chaffee, K. P.; Haddad, T. S.; Romo-Uribe, A.; Lichtenhan, J. D. In *Liquid Crystals for Advanced Technologies*; Chen, S., Bunning, T., Eds.; MRS Symposium Proceedings No. 425; MRS: Washington, DC, 1996; p 137.
(55) Furukawa, A.; Lenz, R. W. *Macromol. Chem., Macromol. Symp.* **1986**, *2*, 3.
(56) Kim, S. S.; Han, C. D. *Macromolecules* **1993**, *26*, 3176.
(57) Kim, S. S.; Han, C. D. *Polymer* **1994**, *35*, 93.
(58) Kim, S. S.; Han, C. D. *Macromolecules* **1993**, *26*, 6633.
(59) Global Lab Image is an image analysis software marketed by Data Translation, Inc.
(60) (a) Han, C. D.; Lem, K.-W. *Polym. Eng. Rev.* **1982**, *2*, 135. (b) Chuang, H.-K.; Han, C. D. *J. Appl. Polym. Sci.* **1984**, *29*, 2205. (c) Han, C. D.; Yang, H. H. *J. Appl. Polym. Sci.* **1987**, *33*, 1221. (d) Han, C. D. *J. Appl. Polym. Sci.* **1988**, *35*, 167.
(61) (a) Han, C. D.; Jhon, M. S. *J. Appl. Polym. Sci.* **1986**, *32*, 3809. (b) Han, C. D.; Kim, J. K. *Macromolecules* **1989**, *22*, 4292.
(62) Janeschitz-Kriegl, H. *Polymer Melt Rheology and Flow Birefringence*; Springer-Verlag: Berlin, 1983.
(63) Hall, E.; Ober, C. K.; Kramer, E. J.; Colby, R. H.; Gillmor, J. R. *Macromolecules* **1993**, *26*, 3764.
(64) Han, C. D.; Kim, J. *J. Polym. Sci., Polym. Phys. Ed.* **1987**, *25*, 1741.
(65) Han, C. D.; Kim, J.; Kim, J. K. *Macromolecules* **1989**, *22*, 383.
(66) Han, C. D.; Baek, D. M.; Kim, J. K. *Macromolecules* **1990**, *23*, 561.
(67) Blumstein, R. B.; Stickles, E. M.; Gauthier, M. M.; Blumstein, A. *Macromolecules* **1984**, *17*, 177.
(68) Viney, C.; Donald, A. M.; Windle, A. H. *Polymer* **1985**, *26*, 870.
(69) Dobb, M. G.; Johnson, D. J.; Saville, B. P. *J. Polym. Sci., Polym. Symp.* **1977**, *58*, 237.
(70) Roche, E. J.; Allen, S. R.; Fincher, C. R.; Paulson, C. *Mol. Cryst. Liq. Cryst.* **1987**, *153*, 547.
(71) Meyer, R. B. *Solid State Commun.* **1973**, *12*, 585.

MA970737H